


Article

Mineralogical and Geochemical Composition of Late Permian Coals from Dengfeng Coalfield, North China: Conversion of Clay Minerals in Coal during Coalification

Shuyuan Ning¹, Zhenzhi Wang^{1,*} , Hui Wang², Chunxiang Chen³, Hui Zhao⁴, Bo Huang⁵ and Qiming Zheng⁵

¹ School of Resources and Environment, Henan Polytechnic University, Jiaozuo 454003, China; ningshuyuan81@163.com

² Chinacoal Xindeng Zhengzhou Coal Co., Ltd., Zhengzhou 452477, China; whjxkf68@163.com

³ Henan Academy of Geology, Zhengzhou 450016, China; czw1127@163.com

⁴ No. 1 Geological Team of Shandong Provincial Bureau of Geology and Mineral Resources, Jinan 250014, China; zhwj816@163.com

⁵ School of Environment and Bioengineering, Henan University of Engineering, Zhengzhou 451191, China; hb123_@126.com (B.H.); zqm6502644@163.com (Q.Z.)

* Correspondence: zhenzhiwang@hpu.edu.cn

Abstract: Dengfeng Coalfield represents a significant coalfield in Henan Province, North China. It is therefore essential to gain an understanding of the mineralogy and geochemistry of the Dengfeng coal, both from a geochemical perspective and in terms of the wider environmental context. In this study, a total of 27 coal bench samples were collected from the No. III coal of the Dengfeng Coalfield. The mineral species and major elements were quantitatively analysed using the X-ray diffraction and X-ray fluorescence methods, respectively. The minerals in the Dengfeng coal are dominated by ammonian illite and kaolinite with average contents of 3.73% and 7.47%, respectively. These are followed by calcite (2.74% on average) and ankerite (0.49%). The mean value of the kaolinite Hinkley index, which is a quantitative measure of kaolinite crystallinity, is 1.26. This suggests that kaolinite formation is primarily driven by diagenetic recrystallisation. The ammonian illite exhibits an average d_{001} of 10.2995 Å, indicative of a prevalence of NH_4^+ interlayer cations, with K^+ also present in notable quantities. The ratio of NH_4^+ to $(\text{NH}_4^+ + \text{K}^+)$ has an average value of 0.90, which is indicative of the predominance of NH_4^+ . The mean value of the illite Kübler index, which is a quantitative measure of illite crystallinity, is 0.264. This suggests that the diagenetic conditions correspond to the rank of the Dengfeng coal. The kaolinite present in the Dengfeng coal is suggested to have been derived from terrigenous detritus and subsequently subjected to diagenetic recrystallisation, resulting in a relatively high Hinkley index. The ammonian illite in the Dengfeng coal was predominantly formed through the conversion of the precursor kaolinite, with the influence of seawater during peat accumulation favouring the conversion of kaolinite to ammonian illite.

Keywords: Dengfeng Coalfield; kaolinite; Hinkley index; ammonian illite; Kübler index; conversion of kaolinite to ammonian illite



Citation: Ning, S.; Wang, Z.; Wang, H.; Chen, C.; Zhao, H.; Huang, B.; Zheng, Q. Mineralogical and Geochemical Composition of Late Permian Coals from Dengfeng Coalfield, North China: Conversion of Clay Minerals in Coal during Coalification. *Processes* **2024**, *12*, 1688. <https://doi.org/10.3390/pr12081688>

Academic Editor: Carlos Sierra Fernández

Received: 17 July 2024

Revised: 9 August 2024

Accepted: 10 August 2024

Published: 13 August 2024



Copyright: © 2024 by the authors. Licensee MDPI, Basel, Switzerland. This article is an open access article distributed under the terms and conditions of the Creative Commons Attribution (CC BY) license (<https://creativecommons.org/licenses/by/4.0/>).

1. Introduction

Coal is the most abundant and widely distributed fossil fuel in the world. In comparison to other fossil fuels, it is also the easiest energy resource to use. As a clastic rock with significant organic carbon content, coal is composed of highly complex components, with inorganic minerals representing a crucial element [1–3]. The minerals present in coal can be broadly classified into several categories, including aluminosilicates, carbonates, sulfides, oxides, and sulfate minerals. Among these, the aluminosilicates are the most prevalent mineral group, comprising predominantly clay minerals [4–6].

The most prevalent clay mineral in coal is kaolinite, followed by illite–smectite interstratified mineral, illite, chlorite, paragonite, margarite, pyrophyllite, rectorite, chlorite–smectite interstratified mineral, etc. [4,5]. The occurrence, formation and conversion of clay minerals reflect certain geological processes, including a peat accumulation environment, marine transgression, hydrothermal fluid circulation, volcanic ash deposition and coalification. These geological processes have significant effects on the species, content and mode of occurrence of the clay minerals [7–11]. Dai et al. [9,12] systematically studied the minerals and trace elements in Chinese coal, suggested that a range of factors, including hydrothermal fluid, groundwater, volcanic ash, sediment source and depositional environment, can influence the enrichment of clay minerals in coal. Zhao et al. [13] conducted a study of the minerals present in coal deposits in the Sydney Basin, Australia, which had been influenced by volcanism. The results indicated that the minerals mainly included illite–smectite interstratified minerals, kaolinite, quartz, K-feldspar and siderite. Chen et al. [14] reported the occurrence of authigenic chlorite, serpentinite and muscovite in coal influenced by magmatic hydrothermal fluids. Zhang et al. [15] reported that kaolinite and illite may have derived from the weathering of feldspar and mica, and authigenic kaolinite occurred as cell fillings and epigenetic illite occurred as fracture fillings in macerals. In addition, the minerals in coal have certain influence on the atmospheric ecological environment. The minerals in coal are the precursors of the dust and fly ash generated during coal mining and combustion, which have considerable influence on the atmospheric environment and public health [16–18]. Therefore, the study of the minerals in coal is necessary and significant from a geological and environmental point of view.

A number of studies have focused on the mineralogy and geochemistry of Carboniferous–Permian coals in the North China Coal Basin [1,7–13,15], but the study of the mineralogy and geochemistry of coals in the West Henan Mining District, which is a major part of the North China Coal Basin, is relatively weak. Therefore, in this study, coal samples were collected from Dengfeng Coalfield, a major coal field in West Henan Mining District, and the contents of various minerals and major element oxides in the coal samples were detected by X-ray diffraction (XRD) and X-ray fluorescence (XRF) methods, respectively. The X-ray diffraction (XRD) characteristics of the clay minerals in coal were calculated according to the XRD patterns of the coal samples. Thereafter, the XRD and X-ray fluorescence (XRF) data were quantitatively compared in order to estimate the modes of occurrence of the major elements in the coal samples. The objectives of this study are to investigate the source and formation of the clay minerals in the Dengfeng coal, as well as the conversion between the clay minerals themselves. Furthermore, the study seeks to identify the geological processes that have shaped the formation and conversion of the clay minerals.

2. Geological Setting

The Dengfeng Coalfield is located in the southern region of the China North Coal Basin, covering an area of 1217 km² (Figure 1). The coal-bearing strata in the Dengfeng Coalfield are situated in the Carboniferous Taiyuan and Permian Shanxi formations, with average thicknesses of 56.32 m and 82.05 m, respectively [19] (Figure 2). The Carboniferous Taiyuan formation is in conformable contact with the underlying Carboniferous Benxi formation and comprises predominantly dark grey limestone, mudstone, sandy mudstone, siltstone and coal, as well as fine-grained sandstone and carbonaceous mudstone. The Carboniferous Taiyuan Formation comprises 12 coal seams, none of which are currently minable. The Permian Shanxi Formation is in conformable contact with the Taiyuan Formation and is primarily composed of light grey and grey mudstone, sandy mudstone, siltstone, and fine-grained and medium-grained sandstone and coal, as well as carbonaceous mudstones. The Permian Shanxi Formation comprises six coal seams, of which only No. II1 Coal is minable. The stratum that overlies the Shanxi Formation is the non-coal-bearing Permian Lower Shihezi Formation [19,20]. The II1 Coal was accumulated on the tidal flat of a lagoon shore, and a large-scale marine transgression followed the peat accumulation of the II1

Coal. This indicates that the No. II1 Coal was significantly influenced by seawater during and after peat accumulation [21].

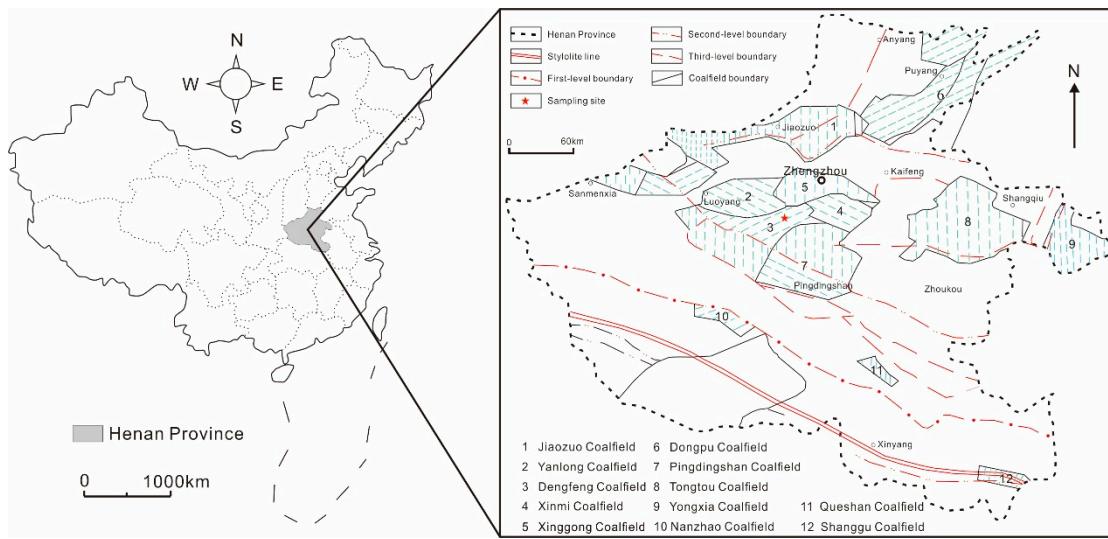


Figure 1. Location of the Dengfeng Coalfield and sampling sites in the coalfield (modified from Liu [21]).

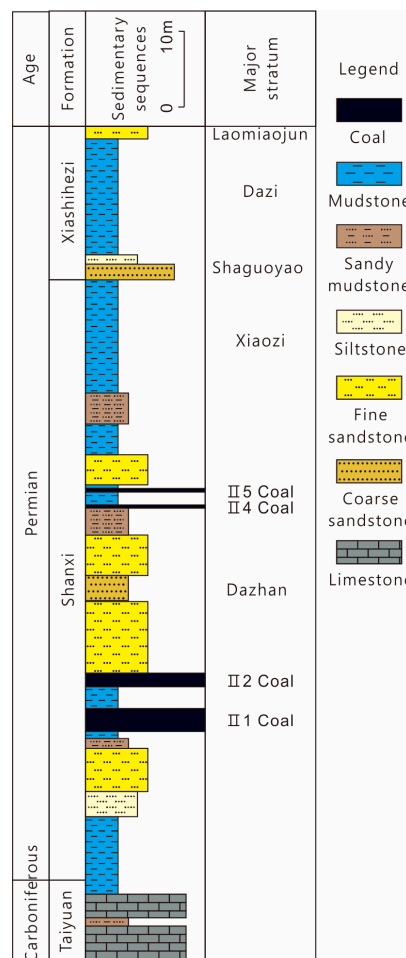


Figure 2. Stratigraphy of the Dengfeng Coalfield and the sampled coal seam (modified from Lin [22]).

3. Samples and Analytical Procedures

3.1. Sample Collection

In this study, sampling took place in the Xindeng Coal Mine in Dengfeng Coalfield, North China, and the sampling coal seam is the No. II1 Coal, with an average thickness of 4.05 m. According to the procedure outlined in Chinese Standard Method GB/T 482-2008 [23], a total of 27 coal bench samples were collected from the sampling coal mine, extending from the footwall to the hanging wall. Each coal bench was cut to a thickness of 0.15 m over an area measuring 10 cm in width and 10 cm in depth. No parting was obtained from this coal seam. The sample numbers of coal benches are XD-21-C1 to XD-21-C28, with the exception of XD-21-C27. Once collected, all of the coal benches were immediately stored in plastic bags to avoid contamination and deliquescence.

3.2. Ash Yield and Volatile-Matter Analysis

In accordance with the standards set forth by the American Society for Testing and Materials (ASTM) in Standards D3174-04 and D3175-02 [24,25], the ash yield on a dry basis (A_d) and volatile matter on a dry and ash-free basis (V_{daf}) of the coal samples were determined in this study.

3.3. X-ray Diffraction (XRD) Analysis

The coal bench samples were subjected to crushing and grinding with a final particle size of <200 μm , in preparation for the subsequent analysis. The minerals in the coal samples were identified by X-ray diffraction (XRD) analysis, which was performed by a D/max-2500/PC powder diffractometer. The operating conditions were as follows: power, 4 kW (40 kV, 100 mA); scanning speed, 4°/min; step, 0.02°; div slit, 1°; and rec slit, 0.3 mm. The XRD pattern was recorded over a 2 θ interval of 2.5–45° for each coal sample. The proportion of each mineral in the coal samples was quantitatively calculated using Quan software 1.0 which is developed by Lin [20] according to the method proposed by Chung et al. [26–28] and outlined in the Chinese Petroleum and Gas Industry Standard Method SY/T 5163-2010 [29].

Liu and Zheng conducted a comprehensive study of the minerals in the coal seam in North China [8]. The general chemical compositions of the minerals identified were cited from the reports of Liu and Zheng and are presented in Table 1 [8]. In consideration of the mineral proportions and the general chemical compositions of the minerals, the loss on ignition (815 °C) of the total minerals for each coal sample can be calculated as follows:

$$LOI = P_{Illt} \times (M_{H_2O} + 0.45 \times M_{(NH_4)_2O}) / M_{Illt} + P_{Kln} \times 4 \times M_{H_2O} / M_{Kln} + P_{Cal} \times M_{CO_2} / M_{Cal} + P_{Ank} \times (2 \times M_{CO_2} - 0.375 \times M_O) / M_{Ank} \quad (1)$$

The M_{Illt} , M_{Kln} , M_{Cal} and M_{Ank} were used to represent the molar mass (g/mol) of the illite, kaolinite, calcite and ankerite, respectively. The symbols M_{H_2O} , $M_{(NH_4)_2O}$, M_{CO_2} and M_O represent the molar mass (g/mol) of the H_2O , $(NH_4)_2O$, CO_2 and O , respectively. The P_{Illt} , P_{Kln} , P_{Cal} and P_{Ank} represent the proportions (%) of the illite, kaolinite, calcite and ankerite, respectively. The LOI represented the loss on ignition (%) of the total minerals for each coal sample. According to the LOI and A_d of each sample, the total mineral matter content (MC , %) in each coal sample can be calculated as follows:

$$MC = A_d / (1 - LOI) \quad (2)$$

3.4. X-ray Fluorescence (XRF) Analysis

The content of each major elemental oxide in the high-temperature ash (815 °C) of the coal samples was determined by X-ray fluorescence (XRF; ARL ADVANT'XP+) spectrometry, according to the methods outlined by Dai et al. [30]. Major oxides include SiO_2 , Al_2O_3 , TiO_2 , Fe_2O_3 , MgO , CaO , Na_2O and K_2O . Based on a set of fundamental parameters and unique algorithms, a “standard-less” methodology called Uniquant (Version 5.46) was used

for matrix correction and calibration of the XRF data. The content of each major element oxide was obtained according to the XRF results and A_d .

Table 1. Chemical compositions of the minerals in the Dengfeng coal samples (Cited from Liu and Zheng [8]).

| Mineral | Chemical Composition | Ratio |
|---------|---|---|
| Qz | SiO ₂ | / |
| Illt | (NH ₄) _{0.90} K _{0.10} Al ₁₂ (AlSi ₃ O ₁₀)(OH) ₂ | SiO ₂ /Al ₂ O ₃ = 1.18 |
| Kln | Al ₄ Si ₄ O ₁₀ (OH) ₈ | SiO ₂ /Al ₂ O ₃ = 1.18 |
| Cal | CaCO ₃ | / |
| Ank | Ca(Fe _{0.75} , Mg _{0.25})(CO ₃) ₂ | / |
| Ant | TiO ₂ | / |

4. Results

4.1. Ash Yield and Volatile Matter

The A_d of the Dengfeng coals varies from 6.32% to 30.29%, with an average of 12.00% (Table 2). According to the Chinese Standard Method GB/T 15224.1-2004 [31], the Dengfeng coal is classified as an extra-low-to-low-ash coal. The V_{daf} of the Dengfeng coals varies from 11.2% to 15.2%, with an average of 13.09%. According to classification outlined in ASTM 388-99 [32], the Dengfeng coal is classified as an anthracite-grade coal.

Table 2. Mineral proportion and content of the minerals in the Dengfeng coal samples, as well as the A_d , V_{daf} and LOI of the Dengfeng coal samples.

| Sample | A_d | V_{daf} | Mineral Proportion/% | | | | | | LOI | Mineral Content/% | | | | | | |
|-----------|-------|-----------|----------------------|-------|-------|-------|-------|------|-------|-------------------|------|-------|-------|------|-------|------|
| | | | Qz | Kln | Cal | Ank | Illt | Ant | | MC | Qz | Kln | Cal | Ank | Illt | Ant |
| XD-21-C1 | 15.34 | 11.4 | 6.04 | 17.9 | 60.01 | 8.43 | 7.48 | 0.14 | 33.04 | 22.91 | 1.38 | 4.10 | 13.75 | 1.93 | 1.71 | 0.03 |
| XD-21-C2 | 30.29 | 13.3 | 14.01 | 43.85 | 7.62 | 1.39 | 32.14 | 1 | 13.53 | 35.03 | 4.91 | 15.36 | 2.67 | 0.49 | 11.26 | 0.35 |
| XD-21-C3 | 13.43 | 13.1 | 1.81 | 45.22 | 35.08 | 9.45 | 7.75 | 0.69 | 26.32 | 18.23 | 0.33 | 8.24 | 6.39 | 1.72 | 1.41 | 0.13 |
| XD-21-C4 | 28.9 | 14.5 | 0 | 42.47 | 7.46 | 1.3 | 47.06 | 1.71 | 14.86 | 33.94 | 0.00 | 14.42 | 2.53 | 0.44 | 15.97 | 0.58 |
| XD-21-C5 | 10.83 | 15.2 | 0 | 44.35 | 34.11 | 9.97 | 10.49 | 1.07 | 26.27 | 14.69 | 0.00 | 6.51 | 5.01 | 1.46 | 1.54 | 0.16 |
| XD-21-C6 | 14.52 | 13.1 | 0 | 23.29 | 47.28 | 5.21 | 23.19 | 1.03 | 28.64 | 20.35 | 0.00 | 4.74 | 9.62 | 1.06 | 4.72 | 0.21 |
| XD-21-C7 | 17.94 | 14.5 | 0 | 54.97 | 6.96 | 2.47 | 32.71 | 2.89 | 15.28 | 21.18 | 0.00 | 11.64 | 1.47 | 0.52 | 6.93 | 0.61 |
| XD-21-C8 | 9.99 | 11.2 | 0 | 16.36 | 60.15 | 16.74 | 5.75 | 1 | 35.98 | 15.60 | 0.00 | 2.55 | 9.39 | 2.61 | 0.90 | 0.16 |
| XD-21-C9 | 6.72 | 13.4 | 0 | 52.7 | 3.49 | 4.56 | 38.45 | 0.79 | 14.89 | 7.90 | 0.00 | 4.16 | 0.28 | 0.36 | 3.04 | 0.06 |
| XD-21-C10 | 7.62 | 14.1 | 0 | 27.33 | 41.15 | 8.08 | 21.89 | 1.56 | 27.50 | 10.51 | 0.00 | 2.87 | 4.32 | 0.85 | 2.30 | 0.16 |
| XD-21-C11 | 6.32 | 13.9 | 0 | 45.08 | 20 | 3.55 | 30.37 | 1.01 | 19.81 | 7.88 | 0.00 | 3.55 | 1.58 | 0.28 | 2.39 | 0.08 |
| XD-21-C12 | 8.93 | 14.2 | 0 | 43.96 | 10.16 | 1.39 | 43.17 | 1.33 | 15.87 | 10.61 | 0.00 | 4.67 | 1.08 | 0.15 | 4.58 | 0.14 |
| XD-21-C13 | 11.77 | 14.8 | 0 | 34.97 | 17.13 | 3.12 | 43.4 | 1.38 | 18.39 | 14.42 | 0.00 | 5.04 | 2.47 | 0.45 | 6.26 | 0.20 |
| XD-21-C14 | 8.48 | 12.1 | 0 | 43.08 | 15.11 | 1.84 | 38.86 | 1.11 | 17.63 | 10.29 | 0.00 | 4.44 | 1.56 | 0.19 | 4.00 | 0.11 |
| XD-21-C15 | 6.88 | 12.9 | 0 | 58.81 | 24.36 | 0 | 16.56 | 0.27 | 20.73 | 8.68 | 0.00 | 5.10 | 2.11 | 0.00 | 1.44 | 0.02 |
| XD-21-C16 | 7.8 | 12.3 | 0 | 51.18 | 8.23 | 1.26 | 38.35 | 0.98 | 15.45 | 9.23 | 0.00 | 4.72 | 0.76 | 0.12 | 3.54 | 0.09 |
| XD-21-C17 | 7.64 | 11.9 | 0 | 58.1 | 9.08 | 0 | 32.11 | 0.72 | 15.61 | 9.05 | 0.00 | 5.26 | 0.82 | 0.00 | 2.91 | 0.07 |
| XD-21-C18 | 10.15 | 11.6 | 0 | 65.48 | 7.47 | 0 | 26.06 | 0.99 | 15.27 | 11.98 | 0.00 | 7.84 | 0.89 | 0.00 | 3.12 | 0.12 |
| XD-21-C19 | 9.79 | 12.1 | 0 | 37.91 | 3.3 | 0.75 | 56.67 | 1.37 | 13.23 | 11.28 | 0.00 | 4.28 | 0.37 | 0.08 | 6.39 | 0.15 |
| XD-21-C20 | 8.93 | 12.3 | 0 | 71.39 | 3.32 | 0 | 24.49 | 0.81 | 14.10 | 10.40 | 0.00 | 7.42 | 0.35 | 0.00 | 2.55 | 0.08 |
| XD-21-C21 | 13.01 | 12.2 | 0 | 80.25 | 2.39 | 0 | 15.77 | 1.59 | 13.97 | 15.12 | 0.00 | 12.14 | 0.36 | 0.00 | 2.38 | 0.24 |
| XD-21-C22 | 14.84 | 13.4 | 0 | 79.31 | 1.62 | 0 | 17.51 | 1.57 | 13.69 | 17.19 | 0.00 | 13.64 | 0.28 | 0.00 | 3.01 | 0.27 |
| XD-21-C23 | 10.06 | 13.5 | 0 | 67.2 | 11.72 | 3.68 | 15.32 | 2.08 | 17.66 | 12.22 | 0.00 | 8.21 | 1.43 | 0.45 | 1.87 | 0.25 |
| XD-21-C24 | 10.55 | 13.1 | 0 | 76.23 | 17.2 | 0 | 4.8 | 1.77 | 18.73 | 12.98 | 0.00 | 9.90 | 2.23 | 0.00 | 0.62 | 0.23 |
| XD-21-C25 | 11.71 | 12.9 | 0 | 94.43 | 0 | 0 | 4.28 | 1.3 | 13.64 | 13.56 | 0.00 | 12.80 | 0.00 | 0.00 | 0.58 | 0.18 |
| XD-21-C26 | 11.01 | 13.1 | 0 | 47.21 | 17 | 0 | 35.73 | 0.06 | 17.97 | 13.42 | 0.00 | 6.34 | 2.28 | 0.00 | 4.80 | 0.01 |
| XD-21-C28 | 10.58 | 13.2 | 0 | 96.25 | 0 | 0 | 3.05 | 0.69 | 13.76 | 12.27 | 0.00 | 11.81 | 0.00 | 0.00 | 0.37 | 0.08 |
| Av | 12.00 | 13.09 | 0.81 | 52.57 | 17.46 | 3.08 | 24.94 | 1.14 | 18.96 | 14.85 | 0.25 | 7.47 | 2.74 | 0.49 | 3.73 | 0.18 |

Av, average; LOI , loss on ignition, calculated from the A_d , mineral proportions and mineral chemical compositions.

4.2. Mineral Proportions and Contents

According to the XRD results, the identified minerals in the coal samples are dominated by clay and carbonate minerals, followed by oxide minerals (Table 2). The clay minerals include kaolinite and ammonian illite as indicated by the XRD patterns, with average

proportions of 52.57% and 24.94%, respectively. The ammonian illite has interlayer cations dominated by NH_4^+ followed by K^+ [33,34]. The carbonate minerals, namely calcite and ankerite, were identified in the XRD patterns of the majority of coal samples, with average proportions of 17.46% and 3.08%, respectively. The oxide minerals include quartz and anatase. Anatase was found to have an average proportion of 1.14%, while the quartz was only identified in the uppermost coal samples of the coal seam, with an average proportion of 0.81%.

The calculation results for the contents of the minerals in Dengfeng coal samples are shown in Table 2. The total mineral matter contents of the coal samples range from 7.88% to 35.03%, with an average of 18.96%. The two most abundant minerals were illite (3.73% on average) and kaolinite (7.47%), followed by calcite (2.74%) and ankerite (0.49%).

4.3. Contents of the Major Element Oxides

The contents of the major element oxides in the coal samples are listed in Table 3. The two most abundant major element oxides, SiO_2 and Al_2O_3 , exhibit fluctuations between 0.94% and 59.45% and 0.76% and 19.96%, with respective averages of 7.23% and 4.38%. Other major element oxides include CaO (1.66% on average), Fe_2O_3 (0.14%), TiO_2 (0.18%), MgO (0.026%), K_2O (0.022%) and Na_2O (0.003%). The SiO_2 , Al_2O_3 , Na_2O , K_2O , MgO, Fe_2O_3 and TiO_2 contents of the Dengfeng coal are relatively lower than the Chinese average coal, which can be mainly attributed to the low A_d of the Dengfeng coal. However, the presence of calcite and ankerite in the Dengfeng coal results in a higher CaO content than that observed in the Chinese average coal. The $\text{SiO}_2/\text{Al}_2\text{O}_3$ ratio of the Dengfeng coal shows an average of 1.36, which is higher than the $\text{SiO}_2/\text{Al}_2\text{O}_3$ ratios of the kaolinite and illite reported by Liu and Zheng [8] (Table 1). This suggests that the Si/Al number ratio was higher than 1:1, indicating that ammonian illite did not fully convert to tobelite [33].

Table 3. Major element oxide contents (in wt%) of the Dengfeng coal samples, as well as $\text{SiO}_2/\text{Al}_2\text{O}_3$ and K values of the Dengfeng coal samples.

| Sample | SiO_2 | Al_2O_3 | Na_2O | K_2O | CaO | MgO | Fe_2O_3 | TiO_2 | $\text{SiO}_2/\text{Al}_2\text{O}_3$ | $\text{Al}_2\text{O}_3/\text{TiO}_2$ | K |
|--------------------|----------------|-------------------------|-----------------------|----------------------|------|------|-------------------------|----------------|--------------------------------------|--------------------------------------|-------|
| XD-21-C1 | 4.15 | 2.34 | 0.01 | 0.01 | 8.19 | 0.14 | 0.47 | 0.03 | 1.78 | 73.07 | 1.357 |
| XD-21-C2 | 17.43 | 10.64 | 0.01 | 0.09 | 1.62 | 0.02 | 0.14 | 0.34 | 1.64 | 30.91 | 0.063 |
| XD-21-C3 | 4.82 | 3.81 | 0.01 | 0.02 | 4.04 | 0.09 | 0.52 | 0.13 | 1.26 | 30.49 | 0.539 |
| XD-21-C4 | 16.18 | 10.45 | 0.01 | 0.04 | 1.51 | 0.02 | 0.12 | 0.57 | 1.55 | 18.32 | 0.062 |
| XD-21-C5 | 3.87 | 3.09 | 0.01 | 0.00 | 3.19 | 0.06 | 0.45 | 0.16 | 1.25 | 19.69 | 0.531 |
| XD-21-C6 | 4.80 | 3.52 | 0.00 | 0.02 | 5.62 | 0.06 | 0.29 | 0.21 | 1.36 | 17.13 | 0.717 |
| XD-21-C7 | 9.08 | 7.07 | 0.00 | 0.05 | 0.96 | 0.03 | 0.13 | 0.61 | 1.29 | 11.52 | 0.070 |
| XD-21-C8 | 1.63 | 1.37 | 0.00 | 0.00 | 5.94 | 0.12 | 0.77 | 0.16 | 1.19 | 8.68 | 2.277 |
| XD-21-C9 | 3.69 | 2.58 | 0.00 | 0.01 | 0.25 | 0.02 | 0.11 | 0.06 | 1.43 | 41.52 | 0.060 |
| XD-21-C10 | 2.64 | 1.90 | 0.00 | 0.00 | 2.62 | 0.05 | 0.23 | 0.16 | 1.39 | 11.69 | 0.639 |
| XD-21-C11 | 3.02 | 2.16 | 0.00 | 0.01 | 0.96 | 0.01 | 0.08 | 0.08 | 1.39 | 27.89 | 0.203 |
| XD-21-C12 | 4.70 | 3.36 | 0.01 | 0.03 | 0.64 | 0.01 | 0.04 | 0.14 | 1.40 | 23.84 | 0.086 |
| XD-21-C13 | 5.91 | 3.98 | 0.00 | 0.03 | 1.49 | 0.02 | 0.14 | 0.20 | 1.49 | 20.02 | 0.166 |
| XD-21-C14 | 4.37 | 3.00 | 0.00 | 0.02 | 0.91 | 0.01 | 0.04 | 0.11 | 1.46 | 26.28 | 0.132 |
| XD-21-C15 | 3.21 | 2.46 | 0.00 | 0.00 | 1.17 | 0.00 | 0.00 | 0.02 | 1.31 | 105.87 | 0.208 |
| XD-21-C16 | 4.16 | 3.03 | 0.00 | 0.03 | 0.46 | 0.01 | 0.03 | 0.09 | 1.38 | 34.14 | 0.069 |
| XD-21-C17 | 4.05 | 3.04 | 0.00 | 0.02 | 0.46 | 0.00 | 0.00 | 0.06 | 1.34 | 47.05 | 0.066 |
| XD-21-C18 | 5.42 | 4.09 | 0.00 | 0.01 | 0.50 | 0.00 | 0.00 | 0.12 | 1.33 | 34.42 | 0.053 |
| XD-21-C19 | 5.74 | 3.60 | 0.01 | 0.03 | 0.24 | 0.00 | 0.02 | 0.15 | 1.60 | 23.89 | 0.029 |
| XD-21-C20 | 4.76 | 3.87 | 0.00 | 0.02 | 0.19 | 0.00 | 0.00 | 0.08 | 1.23 | 46.07 | 0.023 |
| XD-21-C21 | 6.81 | 5.70 | 0.00 | 0.04 | 0.21 | 0.00 | 0.01 | 0.24 | 1.19 | 23.68 | 0.017 |
| XD-21-C22 | 7.92 | 6.43 | 0.00 | 0.04 | 0.16 | 0.00 | 0.01 | 0.27 | 1.23 | 23.91 | 0.012 |
| XD-21-C23 | 4.81 | 3.89 | 0.00 | 0.01 | 0.92 | 0.03 | 0.13 | 0.26 | 1.24 | 15.02 | 0.124 |
| XD-21-C24 | 4.94 | 4.11 | 0.01 | 0.00 | 1.25 | 0.00 | 0.00 | 0.23 | 1.20 | 17.50 | 0.139 |
| XD-21-C25 | 6.15 | 5.36 | 0.00 | 0.02 | 0.00 | 0.00 | 0.01 | 0.18 | 1.15 | 29.66 | 0.001 |
| XD-21-C26 | 5.62 | 4.10 | 0.00 | 0.02 | 1.26 | 0.00 | 0.00 | 0.01 | 1.37 | 510.77 | 0.130 |
| XD-21-C28 | 5.60 | 4.86 | 0.00 | 0.02 | 0.00 | 0.00 | 0.01 | 0.09 | 1.15 | 56.03 | 0.001 |
| Av. | 5.76 | 4.22 | 0.00 | 0.02 | 1.66 | 0.03 | 0.14 | 0.18 | 1.36 | 49.22 | |
| Chinese coal | 8.47 | 5.89 | 0.16 | 0.19 | 1.21 | 0.22 | 4.85 | 0.33 | 1.44 | 17.85 | |
| Zhongtiao Old land | 71.61 | 13.19 | 3.34 | 3.22 | 1.27 | 0.95 | 2.02 | 0.46 | 5.43 | 28.86 | |

Av., average; Chinese coal, cited from Chi and Yan [35]; Zhongtiao Old land, cited from Liu [21].

4.4. XRD Characteristics of the Clay Minerals

4.4.1. Ammonian Illite

Ammonian illite is a phyllosilicate mineral, characterised by a 2:1 layer type. Higashi first identified the ammonian illite in the sedimentary rocks in Japan [33]. Ammonian illite has a basal spacing (d_{001}) close to 10.33 Å, which is slightly higher than that observed for potassium illite (10 Å). Juster et al. [34], Dai et al. [30] and Zheng et al. [7] have identified ammonian illite in the coal-bearing strata of Northeast Pennsylvania, USA, in the coal seam of Daqingshan Coalfield, Inner Mongolia, China and in the coal seam of Qinshui Coalfield, North China, respectively. The ammonian illite is characterised by the interlayer cations dominated by NH_4^+ , followed by K^+ . NH_4^+ has a higher ionic radius (0.148 nm) than K^+ (0.133 nm), resulting in the higher d_{001} of ammonian illite relative to potassium illite [8]. This is the standard method for distinguishing between ammonian illite and potassium illite. The ammonian illite in the coals collected from the Dengfeng Coalfield has d_{001} varying from 10.2543 Å to 10.3300 Å, with an average of 10.2995 Å (Table 4 and Figure 3), indicating that NH_4^+ is the dominant cation in the interlayer, rather than K^+ . The d_{002} , d_{003} and d_{004} of the illite in the Dengfeng coal samples are found to be approximately 5.1644 Å, 3.4412 Å and 2.5810 Å, respectively. Additionally, the $d_{001}:d_{002}:d_{003}:d_{004}$ ratio is observed to be approximately 4:3:2:1. The average values of $FWHM_{002}/FWHM_{001}$, $FWHM_{003}/FWHM_{001}$ and $FWHM_{004}/FWHM_{001}$ are all close to 1:1 ($FWHM$, full width at half maximum of the XRD peak, dimensionless unit), which indicates that the ammonian illite in the Dengfeng coal samples is an inter-stratified mineral comprising both potassium illite and ammonian illite. Furthermore, the cations present in each interlayer have an identical NH_4^+/K^+ ratio, as evidenced in References [36–38].

Table 4. XRD parameters of the ammonian illite in the Dengfeng coal samples, as well as $\text{NH}_4^+ / (\text{NH}_4^+ + \text{K}^+)$ of the Dengfeng coal samples.

| Sample | $d_{001}/\text{Å}$ | d_{002}/d_{001} | d_{003}/d_{001} | d_{004}/d_{001} | $FWHM_{001}$ | $FWHM_{002}/FWHM_{001}$ | $FWHM_{003}/FWHM_{001}$ | $FWHM_{004}/FWHM_{001}$ | $\text{NH}_4^+ / (\text{NH}_4^+ + \text{K}^+)$ |
|-----------|--------------------|-------------------|-------------------|-------------------|--------------|-------------------------|-------------------------|-------------------------|--|
| XD-21-C1 | 10.3055 | | | | 0.267 | | | | 0.92 |
| XD-21-C2 | 10.2969 | 0.49 | | | 0.258 | 0.99 | | | 0.90 |
| XD-21-C3 | 10.31 | 0.50 | | | 0.285 | 0.98 | | | 0.93 |
| XD-21-C4 | 10.2957 | 0.50 | 0.33 | 0.25 | 0.274 | 0.97 | 0.97 | 0.98 | 0.89 |
| XD-21-C5 | 10.3211 | 0.50 | | | 0.277 | 0.99 | | | 0.96 |
| XD-21-C6 | 10.3209 | 0.50 | 0.33 | 0.25 | 0.264 | 1.02 | 1.03 | 1.00 | 0.96 |
| XD-21-C7 | 10.2975 | 0.50 | 0.34 | 0.25 | 0.268 | 0.97 | 1.02 | 1.03 | 0.90 |
| XD-21-C8 | 10.33 | 0.50 | | | 0.257 | 1.08 | | | 0.99 |
| XD-21-C9 | 10.3052 | 0.50 | 0.33 | 0.25 | 0.268 | 0.96 | 0.97 | 0.97 | 0.92 |
| XD-21-C10 | 10.3263 | 0.49 | 0.33 | 0.25 | 0.253 | 1.04 | 1.02 | 1.05 | 0.98 |
| XD-21-C11 | 10.3057 | 0.50 | 0.33 | 0.25 | 0.256 | 1.01 | 1.02 | 1.03 | 0.92 |
| XD-21-C12 | 10.3051 | 0.50 | 0.33 | 0.25 | 0.255 | 1.02 | 1.03 | 1.02 | 0.92 |
| XD-21-C13 | 10.3025 | 0.50 | 0.33 | 0.25 | 0.265 | 0.95 | 0.97 | 1.01 | 0.91 |
| XD-21-C14 | 10.2965 | 0.50 | 0.33 | 0.25 | 0.248 | 1.04 | 1.03 | 1.04 | 0.90 |
| XD-21-C15 | 10.3113 | 0.50 | | | 0.267 | 0.98 | | | 0.94 |
| XD-21-C16 | 10.2902 | 0.50 | 0.33 | 0.25 | 0.262 | 0.95 | 1.04 | 1.05 | 0.88 |
| XD-21-C17 | 10.2965 | 0.50 | 0.33 | 0.25 | 0.276 | 0.99 | 0.97 | 1.00 | 0.90 |
| XD-21-C18 | 10.3016 | 0.50 | 0.34 | 0.25 | 0.257 | 1.04 | 1.03 | 1.02 | 0.91 |
| XD-21-C19 | 10.2869 | 0.50 | 0.33 | 0.25 | 0.256 | 1.00 | 0.99 | 0.97 | 0.87 |
| XD-21-C20 | 10.2972 | 0.51 | | | 0.265 | 0.99 | | | 0.90 |
| XD-21-C21 | 10.2784 | 0.50 | | | 0.271 | 1.01 | | | 0.85 |
| XD-21-C22 | 10.2875 | 0.50 | | | 0.256 | 1.04 | | | 0.87 |
| XD-21-C23 | 10.2997 | 0.50 | | | 0.257 | 1.05 | | | 0.90 |
| XD-21-C24 | 10.299 | | | | 0.268 | | | | 0.90 |
| XD-21-C25 | 10.2581 | | | | 0.259 | | | | 0.79 |
| XD-21-C26 | 10.3063 | 0.50 | 0.33 | 0.25 | 0.268 | 0.96 | 0.99 | 1.00 | 0.92 |
| XD-21-C28 | 10.2543 | | | | 0.258 | | | | 0.78 |
| Sd. | 0.0168 | 0.004 | 0.0034 | 0 | 0.0083 | 0.035 | 0.026 | 0.026 | 0.046 |
| Av. | 10.2995 | 0.50 | 0.33 | 0.25 | 0.264 | 1.00 | 1.01 | 1.01 | 0.90 |

Av., average; Sd., standard deviation.

Pure ammonian illite is characterised by the presence of NH_4^+ as interlayer cations, with a d_{001} value of 10.358 Å [8]. According to the rules of isomorphism, the ammonian illite in this study is a solid solution between pure ammonian illite and pure potassium illite. The d_{001} of the ammonian illite has been observed to increase in conjunction with the $\text{NH}_4^+ / (\text{NH}_4^+ + \text{K}^+)$ ratio in the interlayer. The regression relation for this phenomenon has

been documented by Higashi [33], Drits et al. [37,38] and Zheng et al. [7] and is presented as follows:

$$\text{NH}_4^+ / (\text{NH}_4^+ + \text{K}^+) = 2.786d_{001} - 27.79 \quad (3)$$

In accordance with this equation, the $\text{NH}_4^+ / (\text{NH}_4^+ + \text{K}^+)$ of the ammonian illite in the Dengfeng coal samples was calculated, and the results indicated that $\text{NH}_4^+ / (\text{NH}_4^+ + \text{K}^+)$ varies from 0.78 to 0.99, with an average of 0.90 (Table 4). Kübler (1968) used the $FWHM_{001}$ of the illite (Kübler index, *KI*) to quantify the crystallinity degree [39]. Values between 0.24 and 0.42 $FWHM_{001}$ are indicative of the diagenetic anchizone phenomena, while values >0.24 $FWHM_{001}$ are suggestive of the epizone phenomena [40]. The *KI* of the illite in the Dengfeng coal samples varies from 0.248 to 0.285, with an average of 0.264, indicating a diagenetic environment (Table 4). This is compatible with the rank of the Dengfeng coal samples, which are classified as anthracite-grade coal.

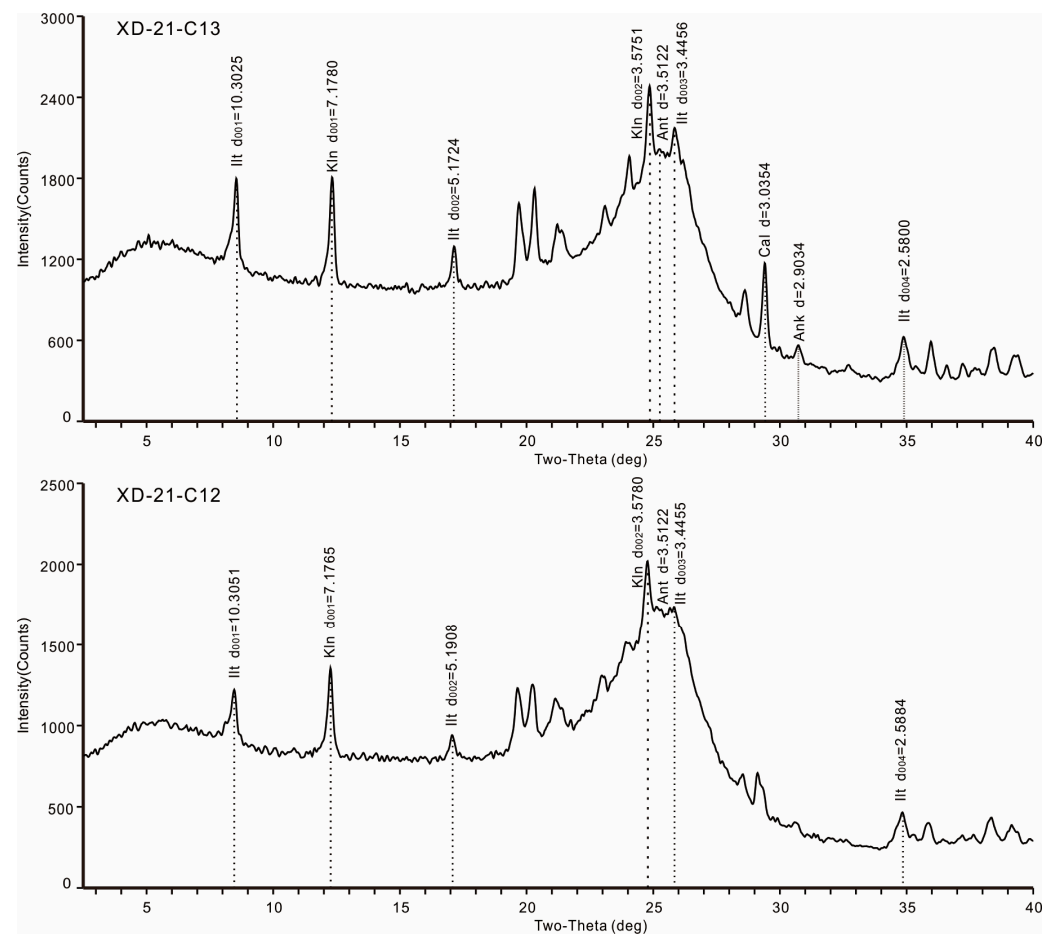


Figure 3. XRD pattern of the Dengfeng coal samples (XD-21-C12 and XD-21-C13). Illt, ammonian illite; Kln, kaolinite; Cal, calcite; Ank, ankerite; Ant, anatase.

4.4.2. Kaolinite

Kaolinite is a common mineral in coal-bearing strata. The crystallinity degree of kaolinite can be quantified using a number of indices, including the Hinkley index (*HI*), the W_C index, the *R2* index and the *AGFI* index [41]. Of these, the *HI* is the mostly frequently-used [41]. Due to the influence of the impact of illite, only W_C can be calculated from the XRD patterns of the coal samples in this study (Table 5 and Figure 3). The W_C was calculated as follows:

$$W_C = W/L1 \quad (4)$$

The W represents the $FWHM$ of the 002 peak, and the $L1$ represents the difference of d_{020} and d_{002} . The W_C of kaolinite in the Dengfeng coal samples varies from 0.203 to 0.307, with an average of 0.251. Zhang et al. provided a summary of the HI and W_C of the kaolinites of different crystallinity degrees [41], and the regression relation between HI and W_C was shown to be as follows:

$$HI = -1.0168W_C + 1.5152$$

The HI index of kaolinite in the Dengfeng coal samples was calculated using the aforementioned equation. The results indicate that the HI index varies from 1.20 to 1.31, with an average of 1.26 (Table 5). Based on the HI index, kaolinite formation can be classified into three types, which include colloidal precipitation with $HI > 1.3$, diagenetic recrystallization with HI ranging between 0.8 and 1.3, and terrigenous detritus with $HI < 0.8$ [8,42]. The formation of kaolinite in the Dengfeng coal samples is predominantly characterised by diagenetic recrystallisation, with colloidal precipitation representing a secondary process.

Table 5. XRD characteristic parameters of the kaolinite in the Dengfeng coal samples.

| Sample | $d_{002}/\text{Å}$ | $d_{020}/\text{Å}$ | $FWHM_{002}$ | W_C | HI |
|-----------|--------------------|--------------------|--------------|--------|-------|
| XD-21-C1 | 3.5813 | 4.4668 | 0.182 | 0.206 | 1.31 |
| XD-21-C2 | 3.5786 | 4.4757 | 0.275 | 0.307 | 1.2 |
| XD-21-C3 | 3.5807 | 4.4705 | 0.221 | 0.248 | 1.26 |
| XD-21-C4 | 3.5751 | 4.4926 | 0.213 | 0.216 | 1.3 |
| XD-21-C5 | 3.5793 | 4.4814 | 0.245 | 0.232 | 1.28 |
| XD-21-C6 | 3.5758 | 4.4936 | 0.222 | 0.242 | 1.27 |
| XD-21-C7 | 3.5787 | 4.4848 | 0.267 | 0.295 | 1.22 |
| XD-21-C8 | 3.5844 | 4.4893 | 0.203 | 0.224 | 1.29 |
| XD-21-C9 | 3.5744 | 4.4913 | 0.208 | 0.227 | 1.28 |
| XD-21-C10 | 3.5787 | 4.4848 | 0.24 | 0.265 | 1.25 |
| XD-21-C11 | 3.5787 | 4.4985 | 0.248 | 0.27 | 1.24 |
| XD-21-C12 | 3.578 | 4.497 | 0.246 | 0.268 | 1.24 |
| XD-21-C13 | 3.5751 | 4.4971 | 0.215 | 0.233 | 1.28 |
| XD-21-C14 | 3.5779 | 4.4969 | 0.192 | 0.209 | 1.3 |
| XD-21-C15 | 3.5759 | 4.4713 | 0.268 | 0.299 | 1.21 |
| XD-21-C16 | 3.5773 | 4.487 | 0.225 | 0.247 | 1.26 |
| XD-21-C17 | 3.5772 | 4.4869 | 0.235 | 0.258 | 1.25 |
| XD-21-C18 | 3.5814 | 4.4759 | 0.242 | 0.271 | 1.24 |
| XD-21-C19 | 3.5786 | 4.4983 | 0.207 | 0.225 | 1.29 |
| XD-21-C20 | 3.5786 | 4.4669 | 0.26 | 0.293 | 1.22 |
| XD-21-C21 | 3.5779 | 4.4704 | 0.244 | 0.273 | 1.24 |
| XD-21-C22 | 3.5785 | 4.4714 | 0.232 | 0.26 | 1.25 |
| XD-21-C23 | 3.5786 | 4.4713 | 0.204 | 0.229 | 1.28 |
| XD-21-C24 | 3.5787 | 4.4714 | 0.213 | 0.239 | 1.27 |
| XD-21-C25 | 3.5813 | 4.4713 | 0.203 | 0.228 | 1.28 |
| XD-21-C26 | 3.5786 | 4.4892 | 0.185 | 0.203 | 1.31 |
| XD-21-C28 | 3.5807 | 4.4657 | 0.265 | 0.299 | 1.21 |
| Sd. | 0.0022 | 0.0111 | 0.0258 | 0.0302 | 0.031 |
| Av. | 3.5785 | 4.4821 | 0.228 | 0.251 | 1.26 |

Av., average; Sd., standard deviation.

4.5. Vertical Variation of the Minerals and Major Element Oxides

The vertical variation of the clay minerals (kaolinite + illite), carbonate minerals (calcite + ankerite), SiO_2 , Al_2O_3 , CaO and Fe_2O_3 are shown in Figure 4. The contents of clay minerals, SiO_2 and Al_2O_3 , have peak values at the same coal benches, which are XD-21-C3 to -C5 at the uppermost part, XD-21-C12 to -C14 at the middle part and XD-21-C21 to -C22 at the lowermost part of the No. III1 Coal seam. The strong correlations of clay minerals with SiO_2 and Al_2O_3 ($r_{\text{clay-SiO}_2} = 0.98$; $r_{\text{clay-Al}_2\text{O}_3} = 0.99$) are compatible with this variation. The contents of the carbonate minerals, CaO and Fe_2O_3 , have peak values at the same coal benches, specifically at XD-21-C1 at the top, XD-21-C6 to -C10 at the middle part, and XD-21-C23 to -C25 at the lowermost part of the No. III1 Coal seam. The strong correlations of carbonate minerals with CaO and Fe_2O_3 ($r_{\text{carbonate-CaO}} = 0.99$; $r_{\text{carbonate-Fe}_2\text{O}_3} = 0.88$) are compatible with this variation. The alternation of the peaks of

clay minerals, SiO_2 and Al_2O_3 , with those of carbonate minerals, CaO and Fe_2O_3 , and the weak correlation between clay and carbonate minerals ($r_{\text{clay-carbonate}} = -0.28$), indicate that clay and carbonate minerals have different sources and formation processes. The studies on the minerals in North China's coal [9,42] suggest that clay minerals are associated with terrigenous detritus, while carbonate minerals are linked to the influence of seawater during peat accumulation.

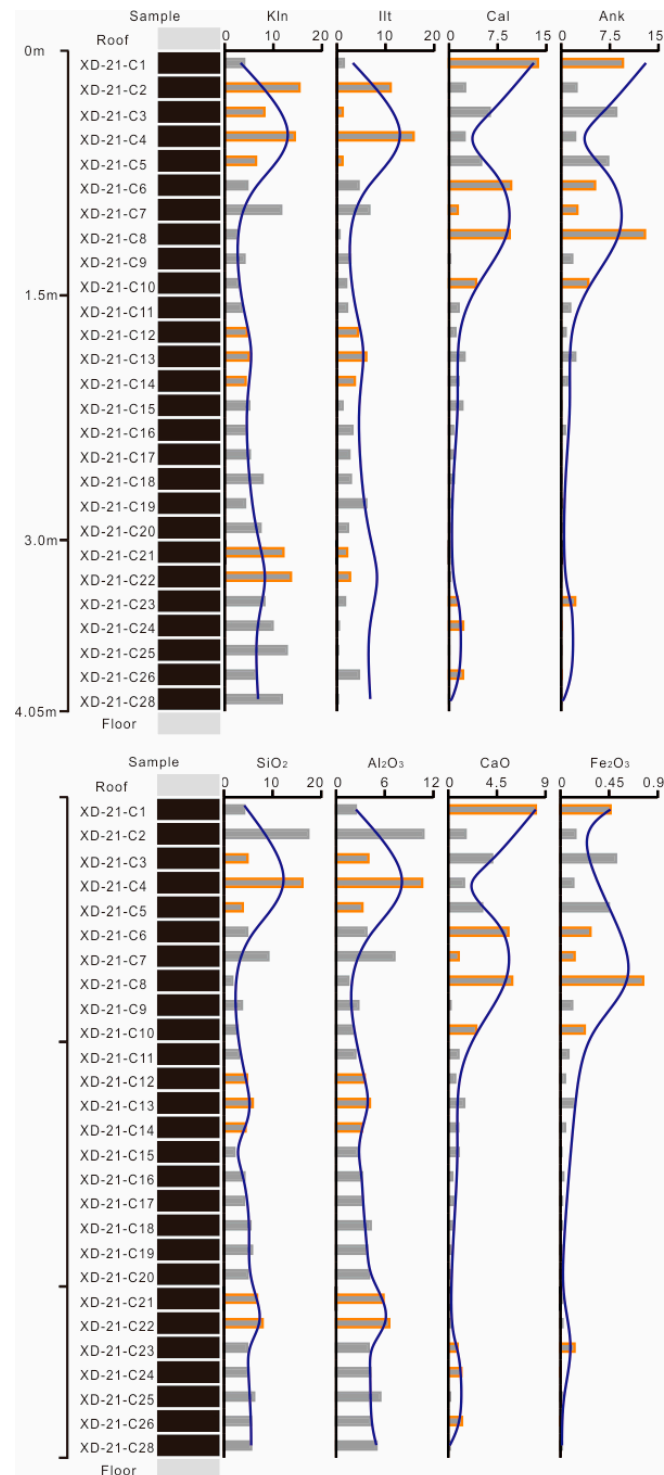


Figure 4. Coal bench samples and vertical variation in the contents of the minerals and major element oxides in the Dengfeng coal samples (orange colour represents high value).

4.6. Modes of Occurrences of the Major Elements

The mineral proportions calculated from the XRD pattern listed in Table 2 and the chemical compositions of the minerals listed in Table 3 can be used to calculate the proportions of SiO_2 , Al_2O_3 , K_2O , CaO , Fe_2O_3 , MgO and TiO_2 in the high-temperature ash (HTA, 815 °C), using the method outlined by Dai et al. [30]. The major element proportions calculated from XRD were normalized and compared with those detected and normalized by XRF using a X-Y plot, with the objective of estimating the modes of occurrence of the major elements in the Dengfeng coal samples (Figure 5). The points in the CaO and TiO_2 plots are observed to fall almost on the diagonal lines, which suggests that Ca in the Dengfeng coal mainly occurs in calcite and ankerite, while Ti is mainly associated with anatase. The points in the MgO and Fe_2O_3 plots are scattered, indicating that the scattered Fe/Mg ratio of the ankerite in the Dengfeng coal samples is slightly higher or lower than that of the ankerite in Table 1 ($\text{Fe}/\text{Mg} = 3$). This may be attributed to the incorporation of Mg and Fe in other mineral phases. The majority of points plotted for SiO_2 fall above the diagonal line, whereas the majority of points plotted for Al_2O_3 fall below the diagonal line. It was inferred that the ammonian illite in the Dengfeng coal samples has a lower Al/Si ratio than that observed in the ammonian illite samples presented in Table 2 ($\text{Al}/\text{Si} = 1$). The Al/Si ratio of the ammonian illite is significantly affected by diagenesis and anchi-metamorphism, with a progressive approach towards a ratio of 1:1 as burial progresses. The majority of points in the K_2O plot fall below the diagonal line, indicating that the ammonian illite in the Dengfeng coal samples has a lower $\text{NH}_4^+ / (\text{NH}_4^+ + \text{K}^+)$ in the interlayer than that of the ammonian illite in Table 1 ($\text{NH}_4^+ / (\text{NH}_4^+ + \text{K}^+) = 0.9$). It can be postulated that the $\text{NH}_4^+ / (\text{NH}_4^+ + \text{K}^+)$ ratio in the interlayer of ammonian illite may approach 1:1, as a consequence of diagenetic and metamorphic evolution [8,40].

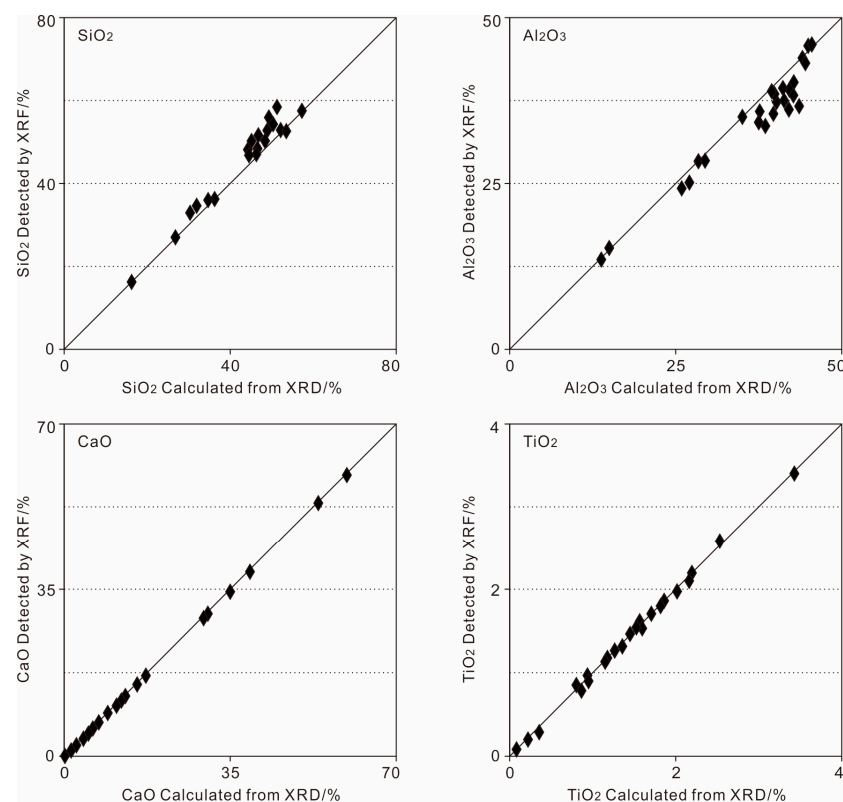


Figure 5. Cont.

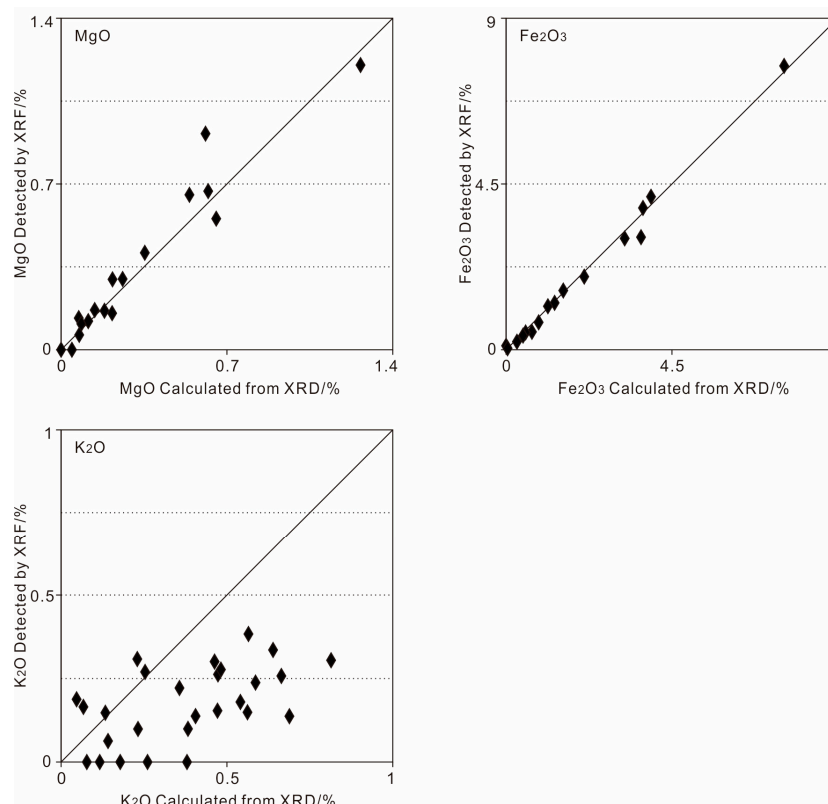


Figure 5. Comparisons between major element oxides calculated from XRD data and those normalized from XRF data.

5. Discussion

5.1. Kaolinite Formation

Kaolinite is a common mineral constituent of coal, and in some cases represents the sole clay mineral present [4,5]. In general, authigenic kaolinite exhibits high crystallinity and is found as cell fillings and fracture fillings in macerals. In contrast, detrital kaolinite displays poor crystallinity. In acidic condition ($\text{pH} < 3$), precursor Al-bearing minerals such as detritus are leached by pore fluid to produce an Al-rich fluid. This then reacts with SiO_2 to form authigenic kaolinite or, when the pH is increased, it crystallises to form Al-rich hydroxide minerals, such as boehmite and diasporite [4,5].

The formation of kaolinite in the Dengfeng coal samples was predominantly the result of diagenetic recrystallisation, followed by colloidal precipitation. The high positive correlation between A_d and kaolinite suggests that the latter is derived from terrigenous detritus (Figure 6). However, kaolinite in the Dengfeng coal samples exhibits a Hildebrand solubility parameter greater than 0.8. This indicates that the detrital kaolinite has been recrystallized during diagenesis, resulting in an increase in crystallinity. When the influence of terrigenous detritus is excluded ($A_d = 0$), the kaolinite content is 1.87%. This fraction of kaolinite is not associated with terrigenous detritus and is inferred to form by colloidal precipitation (authigenic kaolinite). The remaining kaolinite fraction has an average content of 5.60%, representing firstly detritus and then recrystallized kaolinite.

5.2. Conversion of Kaolinite to Ammonian Illite

Ammonian illite is an authigenic mineral [34]. It has been reported that the ammonian illite in coal is mainly formed through the conversion of other clay minerals, including kaolinite and illite–smectite interstratified minerals. The interlayer NH_4^+ is predominantly derived from organic nitrogen or magmatic hydrothermal fluids [7,30]. In this study, the presence of kaolinite and the absence of illite–smectite interstratified mineral and other clay minerals indicates that ammonian illite in the Dengfeng coals samples is mainly formed by

the conversion of kaolinite. The strong correlation of ammonian illite with A_d is compatible with this description ($r_{\text{illite-}A_d} = 0.78$).

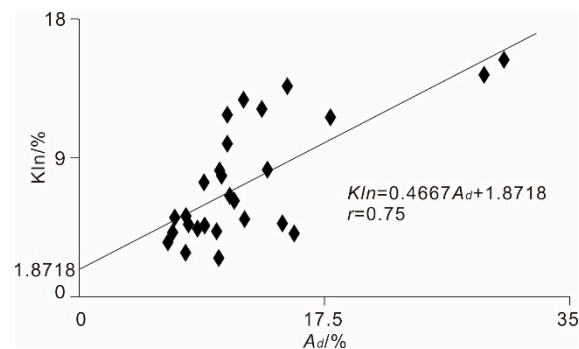


Figure 6. Regression curve of the kaolinite content vs. A_d .

The formation of ammonian illite in coal is significantly influenced by coalification [34]. Ammonian illite is generally identified in high-rank coals (anthracite and low-volatile bituminous), whereas it is absent in low-rank coals. The Dengfeng coal is anthracite-grade coal, corresponding to diagenetic–anchizone conditions. The presence of ammonian illite in the Dengfeng coal samples is consistent with the findings of previous studies [7,30].

The depositional environment also has a significant impact on the formation of ammonian illite. The influence of seawater on peat during the process of peat accumulation is conducive to the preservation of pyrrolic (N-5) and pyridinic (N-6). During coalification, the N-5 and N-6 are released as NH_4^+ , which participates in the conversion of kaolinite to ammonian illite, occurring as interlayer cations [7,43]. In this study, the K value was used to quantify the depositional environment [1], and was calculated as follows:

$$K = (\text{CaO} + \text{MgO} + \text{Fe}_2\text{O}_3) / (\text{SiO}_2 + \text{Al}_2\text{O}_3)$$

The CaO, MgO and Fe_2O_3 are associated with seawater, whereas SiO_2 and Al_2O_3 are associated with terrigenous detritus. Therefore, high and low K values represent seawater and freshwater influences, respectively. The K value of the Dengfeng coal samples exhibits a range of 0.001 to 2.277, with an average of 0.299. The X-Y plot of the K value and the $\text{NH}_4^+ / (\text{NH}_4^+ + \text{K}^+)$ of the ammonian illite indicates that the $\text{NH}_4^+ / (\text{NH}_4^+ + \text{K}^+)$ has an increasing trend as the K value increases (Figure 7). When the K value is less than 0.5, there is a notable increase in the $\text{NH}_4^+ / (\text{NH}_4^+ + \text{K}^+)$ ratio, in conjunction with the K value. Conversely, when the K value is greater than 0.5, the $\text{NH}_4^+ / (\text{NH}_4^+ + \text{K}^+)$ ratio gradually approaches a value of 1.

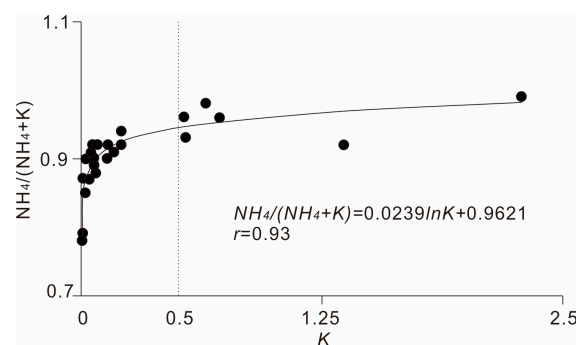


Figure 7. Regression curve of the $\text{NH}_4^+ / (\text{NH}_4^+ + \text{K}^+)$ ratio vs. K value.

6. Conclusions

The total inorganic mineral matter content of the No. II1 coal from the Dengfeng Coalfield exhibits a range of 7.88% to 35.03%, with an average of 14.85%. The most

abundant minerals are ammonian illite (3.73% on average) and kaolinite (7.47%), followed by calcite (2.74%) and ankerite (0.49%).

The d_{001} of the ammonian illite exhibits a range of 10.2543 Å to 10.3300 Å, with an average of 10.2995 Å. This suggests that the interlayer cations are predominantly composed of NH_4^+ , followed by K^+ . The ratio of NH_4^+ to $(\text{NH}_4^+ + \text{K}^+)$ varies from 0.78 to 0.99, with an average of 0.90, which corresponds to the dominance of NH_4^+ in the interlayer. The KI of the ammonian illite varies from 0.248 to 0.285, with an average of 0.264, indicating a diagenetic condition. This is also consistent with the anthracite coal rank of the Dengfeng coal.

The content peak values of clay minerals and carbonate minerals exhibited a periodic alternation along the direction of the coal seam thickness, indicative of disparate sources and formation processes for the two mineralogical groups. The source and formation of the clay minerals are associated with terrigenous detritus, while the formation of carbonate minerals is influenced by seawater during peat accumulation.

The kaolinite present in the Dengfeng coal was derived primarily from terrigenous detritus and subsequently subjected to recrystallisation during the coalification process, resulting in a relatively high HI index (1.26 on average). The ammonian illite was predominantly formed by the conversion of kaolinite during coalification. The observed increase in the $\text{NH}_4^+ / (\text{NH}_4^+ + \text{K}^+)$ ratio, coupled with the elevated K value, suggests that the influence of seawater during peat accumulation facilitated the conversion of other precursor minerals to ammonian illite.

Author Contributions: Methodology, S.N.; software, Z.W.; validation, H.W.; resources, C.C.; writing—original draft, B.H. and Q.Z.; supervision, H.Z. All authors have read and agreed to the published version of the manuscript.

Funding: This study was funded by the National Natural Science Foundation of China (No.42202207), the Major Science and Technology Projects in Xinjiang Uygur Autonomous Region (No. 2023A01004-1) and the Scientific and Technological Project of Henan Province (No. 242102321171).

Data Availability Statement: Data are contained within the article.

Conflicts of Interest: Author Hui Wang was employed by Chinacoal Xindeng Zhengzhou Coal Company. The remaining authors declare that the research was conducted in the absence of any commercial or financial relationships that could be construed as a potential conflict of interest. The company [Chinacoal Xindeng Zhengzhou Coal Company] in affiliation had no role in the design of the study; in the collection, analyses, or interpretation of data; in the writing of the manuscript, or in the decision to publish the results.

References

- Ren, D.; Zhao, F.; Dai, S.; Zhang, J.; Luo, K. *Geochemistry of Trace Elements in Coal*; Science Press: Beijing, China, 2006. (In Chinese)
- Bai, X.; Ding, H.; Lian, J.; Ma, D.; Yang, X.; Sun, N.; Xue, W.; Chang, Y. Coal production in China: Past, present, and future projections. *Int. Geol. Rev.* **2017**, *60*, 535–547. [[CrossRef](#)]
- Zhang, Q. Study on the Environmental Characteristics of Minerals in the Deep Shanxi Formation Coal of the Huainan Coalfield. Mater's Thesis, Anhui University, Hefei, China, 2022. (In Chinese).
- Ward, C.R. Analysis and significance of mineral matter in coal seams. *Int. J. Coal Geol.* **2002**, *50*, 135–168. [[CrossRef](#)]
- Ward, C.R. Analysis, origin and significance of mineral matter in coal: An updated review. *Int. J. Coal Geol.* **2016**, *165*, 1–27. [[CrossRef](#)]
- Finkelman, R.B.; Dai, S.; French, D. The importance of minerals in coal as the hosts of chemical elements: A review. *Int. J. Coal Geol.* **2019**, *212*, 103251. [[CrossRef](#)]
- Zheng, Q.; Liu, Q.; Shi, S. Mineralogy and geochemistry of ammonian illite in intra-seam partings in Permo-Carboniferous coal of the Qinshui Coalfield, North China. *Int. J. Coal Geol.* **2016**, *153*, 1–11. [[CrossRef](#)]
- Liu, Q.; Zheng, Q. *Study on Nitrogen and Nitrogen-Bearing Clay Minerals in Coal Seam*; Science Press: Beijing, China, 2017. (In Chinese)
- Dai, S.; Ren, D.; Chou, C.; Finkelman, R.B.; Seredin, V.V.; Zhou, Y. Geochemistry of trace elements in Chinese coals: A review of abundances, genetic types, impacts on human health, and industrial utilization. *Int. J. Coal Geol.* **2012**, *94*, 3–21. [[CrossRef](#)]
- Dai, S.; Hower, J.C.; Finkelman, R.B.; Graham, I.T.; French, D.; Ward, C.R.; Eskenazy, G.; Wei, Q.; Zhao, L. Organic associations of non-mineral elements in coal: A review. *Int. J. Coal Geol.* **2020**, *218*, 103347. [[CrossRef](#)]

11. Dai, S.; Finkelman, R.B.; French, D.; Hower, J.C.; Graham, I.T.; Zhao, F. Modes of occurrence of elements in coal: A critical evaluation. *Earth-Sci. Rev.* **2021**, *222*, 103815. [[CrossRef](#)]
12. Dai, S.; Zhang, W.; Ward, C.R.; Seredin, V.V.; Hower, J.C.; Li, X.; Song, W.; Wang, X.; Kang, H.; Zheng, L.; et al. Mineralogical and geochemical anomalies of late Permian coals from the Fusui Coalfield, Guangxi Province, southern China: Influences of terrigenous materials and hydrothermal fluids. *Int. J. Coal Geol.* **2013**, *105*, 60–84. [[CrossRef](#)]
13. Zhao, L.; Ward, C.R.; French, D.; Graham, I.T. Mineralogy of the volcanic-influenced Great Northern coal seam in the Sydney Basin, Australia. *Int. J. Coal Geol.* **2012**, *113*, 94–110. [[CrossRef](#)]
14. Chen, X.; Zheng, L.; Jiang, Y.; Jiang, C. Transformation of minerals at the boundary of magma-coal contactzone: Case study from Wolonghu Coal Mine, Huaibei Coalfield, China. *Int. J. Coal Sci. Technol.* **2012**, *8*, 168–175. [[CrossRef](#)]
15. Zhang, N.; Xu, Y.; Ning, S.; Zhao, Y. Mineralogical characteristics in No. 6 coal seam from Xiaohuangshan Coal Mine of Fukang Mining Area, Junggar Coal Field. *Coal Sci. Technol.* **2021**, *49*, 242–250. (In Chinese)
16. Huang, X.; Gordon, T.; Rom, W.N.; Finkelman, R.B. Interaction of Iron and Calcium Minerals in Coals and their Roles in Coal Dust-Induced Health and Environmental Problems. *Rev. Mineral. Geochem.* **2006**, *64*, 153–178. [[CrossRef](#)]
17. Tian, L.; Dai, S.; Wang, J.; Huang, Y.; Ho, S.C.; Zhou, Y.; Lucas, D.; Koshland, C.P. Nanoquartz in Late Permian C1 coal and the high incidence of female lung cancer in the Pearl River Origin area: A retrospective cohort study. *BMC Public Health* **2008**, *8*, 398. [[CrossRef](#)] [[PubMed](#)]
18. Erol, I.; Aydin, H.; Didari, V.; Ural, S. Pneumoconiosis and quartz content of respirable dusts in the coal mines in Zonguldak, Turkey. *Int. J. Coal Geol.* **2013**, *116*, 26–35. [[CrossRef](#)]
19. Chen, S.; Liu, Z.; Deng, Y.; Yao, G. A study on the depositional facies order and control factors of Shanxi Formation Coal Seam thickness at Baiping District, Dengfeng, West Henan. *J. Henan Polytech. Univ. (Nat. Sci.)* **1995**, *14*, 10–18. (In Chinese)
20. Lin, X. *X-ray Diffraction Analytical Technology and Its Geological Application*; Petroleum Industry Press: Beijing, China, 1990; pp. 11–31. (In Chinese)
21. Liu, S. The Coal-Accumulating Environment and Characteristics of Sedimentary Evolution in the Middle Permian Shanxi Formation, Western Henan Province. Master's Thesis, Henan Polytechnic University, Jiaozuo, China, 2010. (In Chinese)
22. Lin, J. Study on Mineralogy and Geochemical Characteristics of Critical Mineral Elements of Coal in Dengfeng Coalfield. Master's Thesis, Hebei University of Engineering, Handan, China, 2022. (In Chinese).
23. *GB/T 482-2008*; Sampling of Coal in Seam. National Standard of P.R. China: Beijing, China, 2008. (In Chinese)
24. *ASTM D 3174-04*; Annual Book of ASTM Standards. Test Method for Ash in the Analysis Sample of Coal and Coke from Coal: Gaseous Fuels. Coal and Coke, ASTM International: West Conshohocken, PA, USA, 2005; Volume 05.06.
25. *ASTM D 3175-02*; Annual Book of ASTM Standards. Test Method for Volatile Matter in the Analysis Sample of Coal and Coke: Gaseous Fuels. Coal and Coke, ASTM International: West Conshohocken, PA, USA, 2005; Volume 05.06.
26. Chung, F.H. Quantitative interpretation of X-ray diffraction patterns of mixtures. I. Matrix-flushing method for quantitative multicomponent analysis. *J. Appl. Crystallogr.* **1974**, *7*, 519–525. [[CrossRef](#)]
27. Chung, F.H. Quantitative interpretation of X-ray diffraction patterns of mixtures. II. Adiabatic principle of X-ray diffraction analysis of mixtures. *J. Appl. Crystallogr.* **1974**, *7*, 526–531. [[CrossRef](#)]
28. Chung, F.H. Quantitative interpretation of X-ray diffraction patterns of mixtures. III. Simultaneous determination of a set of reference intensities. *J. Appl. Crystallogr.* **1975**, *8*, 17–19. [[CrossRef](#)]
29. *SY/T 5163-2010*; Analysis Method for Clay Minerals and Ordinary Non-Clay Minerals in Sedimentary Rocks by the X-ray Diffraction. Petroleum and Gas Industry Standard of P.R. China: Beijing, China, 2010. (In Chinese)
30. Dai, S.; Zou, J.; Jiang, Y.; Ward, C.R.; Wang, X.; Li, T.; Xue, W.; Liu, S.; Tian, H.; Sun, X.; et al. Mineralogical and geochemical compositions of the Pennsylvanian coal in the Adaohai Mine, Daqingshan Coalfield, Inner Mongolia, China: Modes of occurrence and origin of diasporite, gorceixite, and ammonian illite. *Int. J. Coal Geol.* **2012**, *94*, 250–270. [[CrossRef](#)]
31. *GB/T 15224.1-2004*; Classification for Quality of Coal. Part 1: Ash Yield. National Standard of P.R. China: Beijing, China, 2004. (In Chinese)
32. *ASTM D 388-99*; Annual Book of ASTM Standards. Standard Classification of Coals by Rank: Gaseous Fuels. Coal and Coke, ASTM International: West Conshohocken, PA, USA, 2005; Volume 05.06.
33. Higashi, S. Tobelite, a new ammonium dioctahedral mica. *Mineral. J.* **1982**, *11*, 138–146. [[CrossRef](#)]
34. Juster, T.; Brown, P.; Bailey, S. NH₄-bearing illite in very low grade metamorphic rocks associated with coal, northeastern Pennsylvania. *Am. Mineral.* **1987**, *72*, 555–565.
35. Chi, Q.; Yan, M. *Handbook of Elemental Abundance for Applied Geochemistry*; Geological Publishing House: Beijing, China, 2007; pp. 1–148. (In Chinese)
36. Drits, V.A.; Lindgreen, H.; Salyn, A.L. Determination of the content and distribution of fixed ammonium in illite-smectite by X-ray diffraction: Application to North Sea illite-smectite. *Am. Mineral.* **1997**, *82*, 79–87. [[CrossRef](#)]
37. Drits, V.A.; Lindgreen, H.; Sakharov, B.A.; Jakobsen, H.J.; Salyn, A.L.; Dainyak, L.G. Tobelitization of smectite during oil generation in oil source shales. Application to North Sea illite-tobelite-smectite-vermiculite. *Clay Clay Miner.* **2002**, *50*, 82–98. [[CrossRef](#)]
38. Drits, V.A.; Sakharov, B.A.; Salyn, A.L.; Lindgreen, H. Determination of the content and distribution of fixed ammonium in illite-smectite using a modified X-ray diffraction technique: Application to oil source rocks of western Greenland. *Am. Mineral.* **2005**, *90*, 71–84. [[CrossRef](#)]

39. Kübler, B. Évaluation quantitative du métamorphisme par la cristallinité de l'illite. *Cent. Rech. Pau-SNPA Bull.* **1968**, *2*, 385–397.
40. Bayan, M.R.; Hower, J.C. Illite crystallinity and coal metamorphism for selected central Appalachian coals and shales. *Int. J. Coal Geol.* **2011**, *94*, 167–172. [[CrossRef](#)]
41. Zhang, Z.; Xiao, X.; Li, Y.; Xie, J.; Tan, D. Evaluation of the structure order of kaolinite using the X-ray diffraction. *Acta Mineral. Sin.* **2023**, *43*, 97–102. (In Chinese)
42. Liu, Q.; Zhang, P. *Study on Composition and Ore-Forming Mechanism of Kaolinite Rocks in Neopaleozoic Coal-Bearing Strata, North China*; China Ocean Press: Beijing, China, 1997. (In Chinese)
43. Valentim, B.; Guedes, A.; Rodrigues, S.; Flores, D. Case study of igneous intrusion effects on coal nitrogen functionalities. *Int. J. Coal Geol.* **2011**, *86*, 291–294. [[CrossRef](#)]

Disclaimer/Publisher's Note: The statements, opinions and data contained in all publications are solely those of the individual author(s) and contributor(s) and not of MDPI and/or the editor(s). MDPI and/or the editor(s) disclaim responsibility for any injury to people or property resulting from any ideas, methods, instructions or products referred to in the content.